**Supplementary materials**

# Copper Diffusion Rates and Hopping Pathways in Superionic $Cu_2Se$

Sheik Md Kazi Nazrul Islam[1, 2], Prince Mayank[3], Yulou Ouyang[4], Jie Chen[4], Arun. K. Sagotra[5], Meng Li[1], Michael B. Cortie[2], Richard Mole[6], Claudio Cazorla[5], Dehong Yu[6], Xiaolin Wang[1], Robert A. Robinson[1], David Laurence Cortie*[1]

[1] *The Institute for Superconducting and Electronic Materials, Australian Institute for Innovative Materials, University of Wollongong, North Wollongong, NSW 2500, Australia*

[2] *School of Mathematical and Physical Sciences, University of Technology Sydney, Broadway, NSW 2007, Australia*

[3] *Indian Institute of Technology Delhi, New Delhi 110016, India*

[4] *Center for Phononics and Thermal Energy Science, China-EU Joint Lab for Nanophononics, School of Physics Science and Engineering, Tongji University, Shanghai 200092, China*

[5] *School of Materials Science and Engineering, University of New South Wales, Sydney, 2052, Australia*

[6] *The Australian Nuclear Science and Technology Organisation, Lucas Heights, NSW 2232, Australia*

**CORRESPONDING AUTHOR INFORMATION**

Email address: dcortie@uow.edu.au (D. L. Cortie)

## SI1. Technical Details of the DFT *ab-initio* Molecular Dynamics

The temperature in the AIMD simulations was kept fluctuating around a set-point value by using a Nose-Hoover thermostat. Supercells of 3x3x2 $Cu_2Se$ unit cells, containing 216 atoms were used with periodic boundary conditions. Calculations were performed on the RAIJIN supercomputer which is part of the Australian National Computer Infrastructure. Newton's equations of motion were integrated using Verlet's algorithm and a time-step length of 1.5

femtoseconds (fs). Γ-point sampling for integration within the first Brillouin zone was employed. The simulations were equilibrated using 5 ps of run-time, and the total duration of each AIMD production run was for 120 ps.

**SI2. Technical Details of the DFT Nudged Elastic Band Calculations**

Our NEB calculations were performed for large 2x2x2 supercells containing 96 atoms. We used a dense q-point grid of 8x8x8 for first Brillouin zone sampling and an energy plane-wave cut-off of 650 eV.

**SI3. Landmark Analysis of *ab-initio* Molecular Dynamics**

Here we provide a very brief introduction to the concept of landmark analysis for any unfamiliar readers. In the standard approach of molecular dynamics, the atomic positions are written in Cartesian coordinates. While this is straightforward to visualize, it can make certain types of analysis difficult. For example, to analyze ionic hopping or chemical transport, it is desirable to identify when a chemical species has jumped from Site A to Site B. While, in principle, this can be extracted from the derivatives of the Cartesian positions, or by applying spatial thresholds, in practice this is complicated by the noise in the trajectory. Thus, it is generally advantageous to define new variables which depend only on the proximity to predefined landmark positions (e.g. a specific atom, a Voronoi center, a Wyckoff site) and use this to discriminate when jumping events have occurred. To identify the main hopping pathways in the $Cu_2Se$, we first performed an elementary type of landmark analysis by positioning landmarks at every tetrahedral and octahedral interstitial site (labelled as T-sites and O-sites from this point forward). During the trajectory, any Cu that strays within 1 Å of a landmark is tagged with a site ID number and the site type (O or T) belonging to the nearest landmark. If the Cu's site ID number changes, this corresponds to a hopping event, and by tracking the site types it possible to calculate the transition rates for O↔T, O↔O and T↔T transitions. In this way, hopping events and residence times, as well as transition probabilities can be identified. This was implemented using custom-written code in the Visualizing Molecular Dynamics (VMD) software. While the latter approach has the advantage of being simple, it does assume that landmarks can be defined as non-overlapping spheres positioned

judiciously using prior knowledge of the crystal structure. Less biased landmark analysis can also be implemented using more sophisticated mathematics, by performing a decomposition of the Cartesian vectors into a new (non-orthogonal) basis set made of landmark vectors. If the landmark vectors are automatically positioned using Voronoi tessellation, similar landmark vectors can then be clustered automatically to identify special sites based on statistical criteria, and the resulting "site" can have an arbitrary shape. To this end, we also deployed the new SITATOR toolkit developed by Kahle *et al.* for "unsupervised" Voronoi landmark analysis.

**SI4. Partial density of states from the *ab-initio* Molecular Dynamics**

Figure S1 shows the vibrational density of states obtained from *ab-initio* molecular dynamics at 700 K, decomposed into Cu and Se contributions. Figure S2 shows the variation of the total density of states with temperature which shows only a subtle variation.

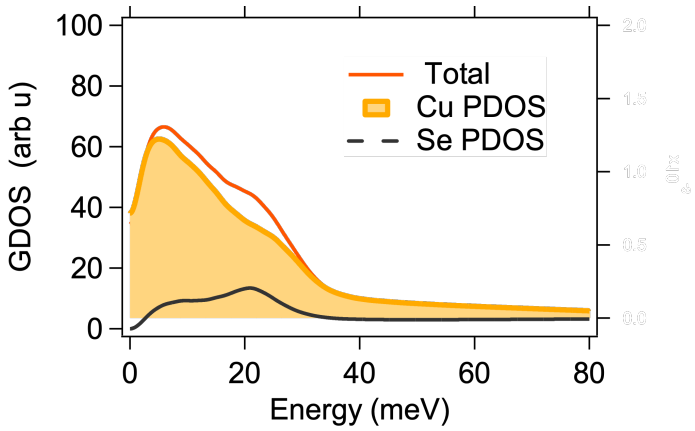


**Figure S1.** Partial density of states of the *ab-initio* molecular dynamics at 700 K

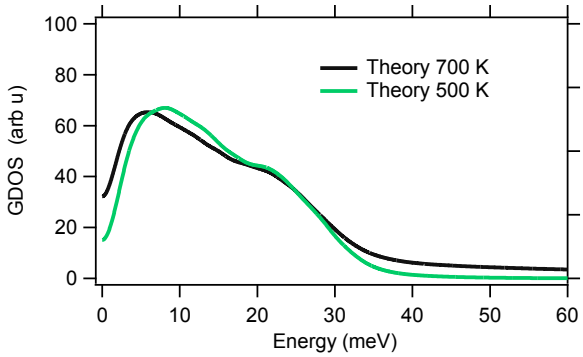

**Figure S2.** Temperature dependence of the DOS extracted from the *ab-initio* molecular dynamics

## SI5. Geometric and Statistical Considerations for Diffusion in the Ideal Fluorite Crystal Structure.

Ideal $Cu_2Se$ crystallizes in the anti-fluorite cubic structure, with the Se ions on a standard face-centered cubic (FCC) Bravais lattice, with lattice constant a. Within this lattice, there are two interstitial sites, a tetrahedral (T) interstitial site at (¼, ¼, ¼), (¼, ¼, ¾) plus FCC translational vectors, and a larger octahedral (O) interstitial site at (½, ½, ½) plus FCC translational vectors. The tetrahedral positions, if fully filled, form a simple-cubic lattice, with lattice constant a/2, and they satisfy the 2:1 stoichiometry of ideal $Cu_2Se$. In contrast, the octahedral positions would support a 1:1 stoichiometry. $Cu_2Se$ is often thought of as a rigid selenium FCC lattice, with relatively mobile Cu ions on the tetrahedral interstitial sites.

The sizes of these interstitial sites, and the Cu-Se bond lengths, assuming that the copper ion would sit at the center of each respective polyhedron, are as listed in Table S1. The octahedral site is clearly larger than the tetrahedral site, but we know from the crystal structure that this is energetically unfavorable and in practice the T-site is the site where the majority of the Cu resides.

**Table S1.** The size of copper sites, and Cu-Se bond-length for the T and O sites in the cubic phase of $Cu_2Se$.

| Interstitial/Vacancy site in ideal FCC lattice | Distance from centre of polyhedron to corners, i.e. Cu-Se bond distance | Number of (triangular) faces | Number of edges | Number of vertices |
|---|---|---|---|---|

| | | | | |
|---|---|---|---|---|
| Tetrahedral at (¼, ¼, ¼) and (¼, ¼, ¾) | √3 a /4 = 0.433 a | 4 | 6 | 4 |
| Octahedral at (½, ½, ½) | a / 2 = 0.5 a | 8 | 12 | 6 |

The FCC lattice can be considered as a network of edge-connected tetrahedra, or equivalently as a network of edge-connected octahedra, Table S2. If a Cu-ion is sitting within a tetrahedron, the most obvious way for it to leave its site is though one of the triangular faces, to one of the four neighboring octahedra (ideally along a [111] direction). It can also move directly from its tetrahedron to one of the 6 edge-connected tetrahedra, passing through the mid-point of one of the edges. This would involve hopping along a [100]-type direction. But these very same edges connect the octahedra to other octahedra (in a direction perpendicular to the direct T-T hop). In other words, the direct O-O hop would take place along [110]-type directions. Hopping through a vertex, would involve a head-on collision with the selenium lattice points, and is therefore very unlikely. In other words, the most open channels in the structure are through the polyhedron faces along [111]-type directions, from T→O or O→T. Less likely are the direct T→T [100]-type or O→O [110]-type hops, though the polyhedron edges. The next-nearest direct T→T hop along [110], which is sometimes discussed in the physics literature, does not pass through any special symmetry points, and involves a short-cut route through the octahedral site. The direct route passes much closer to one of the selenium sites (vertices) and it is therefore energetically unfavorable.

**Table S2.** Geometric considerations for different types of hopping in $Cu_2Se$.

| *Possible hopping routes* | Nearest Cu-Se approach distance, in terms of FCC lattice constant a | Geometry |
|---|---|---|
| T-T, hopping along [100] | a / 2√2 = 0.354 a | through tetrahedral edge |
| T-T, hopping along [110] | a/4 = 0.25 a | No direct path: involves a short-cut through an octahedron |

| | | |
|---|---|---|
| T-O (or O-T) hopping along [111] | a / √6 = 0.408 a | through triangular face |
| O-O, hopping along [110] | a / 2√2 = 0.354 a | through tetrahedral edge, the same as T-T [100], but in the perpendicular direction |

In other words, from a steric point of view, T-O and O-T hops are far more likely than T-T [100] hops, which are in turn more likely than direct T-T [110] hops.

Finally, in the section below we analyze the statistics of finding a vacant tetrahedral site, to which a copper ion can jump. Let us consider non-stoichiometric $Cu_{2-2x}Se$, in which the tetrahedral sites are not all occupied. If any given Cu-ion is going to hop (via an octahedral site) to another tetrahedral site, it can only do so, if the new site is unoccupied. It can jump to any of the four neighboring octahedral which are all unoccupied, but then it has eight options, one for each face of the octahedron:

(a) Jump right back to the tetrahedron, from whence it came

(b) Jump out through one of the three adjacent triangular faces, giving an overall ½ (100)-type hop

(c) Jump out though one of three next-closest triangular faces, giving an overall ½ (110)-type hop

(d) Jump out through the opposite face of the octahedron, giving an overall ½ (111)-type hop

In other words, if the Cu ion makes any given T-O hop, and a fraction x of the tetrahedral sites are unoccupied, the probability of finding a vacant T site to jump onto is 7x (for small x). More precisely, the probability is $1 - (1-x)^7$. Or generalizing to a shell (or sphere) of *n* potential hopping sites, the probability, of finding at least a single vacant site onto which it can hop, is $1 - (1-x)^n$.

But it is more complicated, because the initial T-O hop is one of four such possibilities, and each of these has its own set of (a-d). But some of these go to tetrahedral sites that we have

already considered. In other words, if we consider T→O→T hops, there may be two different routes that the Cu-ion can take (via different octahedral). And for T→O→O→T hops it is yet more complicated.

To simplify the analysis, it is useful to disregard the selenium sublattice, and only count through the occupancies of the shells of Cu-neighbors. The Cu ions sit on a simple cubic lattice, with neighboring Cu ions as listed in Table 3. All hops up to third nearest neighbor are possible via a single O site, and the cumulative probability up to the 3rd neighbors is 23 %. Hopping to the 4th NN and above is not possible via a single O site, and for that reason hops to more distant than the 3rd NN are omitted from Table S3.

**Table S3**. Statistical analysis of the probability of finding a vacancy that is accessible using a T-O transition in $Cu_2Se$.

| Neighbor | Cu-Cu spanning vector (on simple cubic copper lattice) | Accessible through a single octahedral site, T→O→T | Number of neighbors, *n* | Probability of having a neighboring site (in that shell) to hop into, for $Cu_{1.98}Se$ (x = 1% vacancies); $P = 1 - (1-x)^n$ | Cumulative number of neighbours within a shell, $n_S$ | Probability of having a neighboring site (within that shell) to hop into, for $Cu_{1.98}Se$ (x = 1% vacancies); $P = 1 - (1-x)^{ns}$ |
|---|---|---|---|---|---|---|
| 1st Nearest-Neighbor | 100 | yes | 6 | 5.85% | 6 | 5.85% |
| 2ndt Nearest-Neighbor | 110 | yes | 12 | 11.36% | 18 | 16.55% |

| | | | | | | |
|---|---|---|---|---|---|---|
| 3rd NN | 111 | yes (but only half of them) | 8 (only 4 through a single O-site) | 7.73% | 26 (22) | 23.00% |

From this analysis, within the range of possible T → O → T hops (through a single octahedron), it is statistically twice as likely to be a net [110]-type hop, as opposed to a net [100]-type hop: 11.36% compared to 5.85% (for a 1% vacancy probability)

**SI6. Experimental Thermal Conductivity:**

The thermal diffusivity ($D$) was measured by the laser-flash method (Linseis LFA 1000) under vacuum. The assumptions made when using this method include (i) homogeneity and isotropy of the material and (ii) property invariance with temperature within experimental conditions (see ASTM standard E1461 for full detail of technique). The specific heat ($C_p$) was determined by differential scanning calorimetry (DSC) (Netzsch DSC-204F1-Phoenix calorimeter) under an argon atmosphere with a flow rate of 50 ml/min. The sample density (ρ) was calculated using the measured weight and dimensions. The thermal conductivity (κ) was calculated by $= D \times C_p \times \rho$. Note that $D$ is ostensibly depressed during the endothermic α→β phase transition whereas $C_p$ is ostensibly increased. The net result is a spurious value for κ whilst the phase transformation is in progress.

**SI7. Technical Details of Neutron Scattering Experiment**

To account accurately for the slight Q-dependence (angular dependence) of the resolution function, all data were fitted by convoluting with the true resolution function determined by measuring a vanadium standard. The data on the area detector was also normalized per-pixel to the signal from the vanadium standard. Data were collected at 300, 400, 500, 550 and 675 K. The background signal was subtracted using scans of the empty sample can under identical conditions. To permit analysis of the quasielastic component, the Bragg reflections were excluded by removing the corresponding angular ranges on the detector bank. The remaining data were transformed into S(Q,ω) using a sufficiently coarse Q-resolution such

that there are no missing points. Data manipulations and fitting were carried out using the Large Array Manipulation Program (LAMP) [1].

**SI8. Details of the quasi-elastic fitting model**

This section discusses a general and robust model that can place limits on the diffusion coefficients obtained with QENS, and which is generally suitable for superionic conductors. Although this approach sacrifices a small amount of accuracy, it contains the minimal description of the essential physical processes and can be used to place upper and lower bounds on the diffusion coefficient. There are five distinct steps in the fitting process: 1) selection of of appropriate Q/$\omega$ regions 2) establishing the minimal QENS model capturing the two distinct physical processes 3) quantitative fitting 4) extracting the long-range diffusion component 5) placing bounds on the data. Each of these steps is detailed below.

**Selection of Q and $\omega$ regions for fitting:** In a superionic conductor, three types of motion coexist: 1) diffusion of one species, 2) confined diffusion for ions trapped near their stable site undergoing sporadic large displacements, and 3) phonons for the surrounding lattice causing small collective displacements. Disentangling these three factors in a solid-state QENS experiment is non-trivial because the atomic motion seen by neutron scattering in the intensity function $S(Q,\omega)$ is a superposition of all degrees-of-freedom. However, by carefully selecting the $\omega/\mathrm{Q}$ region, it is possible to select regions where the phonons make virtually no contribution and diffusive (QENS) processes dominate. To be specific, low energy acoustic phonons can be minimized by avoiding the Q-regions corresponding to zone centers. The optical phonons, which are present at all Q, are less of an issue since they generally contribute intensity at $\omega$ >> 0 that is easily distinguished from QENS processes ($\omega \sim 0$). However, in rare cases, low-energy optical modes can still provide a broad background signal, which can be mistaken for a broad quasielastic component. Thus, it is advisable to avoid any contribution of optical phonons by disregarding $\omega$ energies near to and above the first optical branch. Identifying the strong coherent contributions in the simulated cross-section (e.g. Fig. 6(b)) is a good method to cross-check these choices. Thus, in $Cu_2Se$, fitting was accomplished by using data for 0.5 $Å^{-1}$ < Q < 1.6 $Å^{1}$ away from the

Brillouin zone centers, and at energies < 5 meV, below the first optical branches. This prevents spuriously inferring a QENS signal from low energy phonons.

**Establishing the minimum QENS model:** Having restricted the $\omega/Q$ range, the next task is to separate the confined and long-range diffusion components via their unique $Q$ dependence and energy-width. Confined diffusion involves the atom jumping around sporadically, but always eventually returning to the same site, owing to confinement. This generates an elastic component, together with a QENS component. The latter is generally tied to higher frequency vibrations thus giving a broader E-width described by a FWHM ($\Gamma$ >2-10 meV) with an FWHM ($\Gamma$) that is independent of Q (to a very good approximation). In contrast, long-range diffusion involves atoms leaving their initial site, and travelling long distances in the lattice. This leads to a Q-dependent FWHM ($\Gamma$ that increases as $Q^2$, at low momentum transfer, with a $\Gamma$ that is typically in the range of 0.01 - 2 meV below Q = 2.0 $Å^{-1}$. In general the two types of diffusion have very different time-scales, and long-range diffusion involves lower frequency events as many trial hops occur before each long-range hop. To account for these two types of motion, it is generally necessary to use multiple Lorentzians to fit the QENS data. As shown in Figure S3, models fitting to a single Lorentzian yielded unsatisfactory results are reported by others [3, 8, 9], since it yields a convoluted average of the two processes, and the diffusion coefficient obtained will be unreliable. The single Lorentzian fit tends to overestimate the intensity near the elastic line and also fails to capture the higher energy region, leading to a large residue and a poor figure of merit ($\chi^2$). As discussed above, there is also good physical justification for expecting at least two components in the self-correlations, reflected in two (or more) distinct Lorentzian contributions to the QENS. In the case of $Cu_2Se$, two Lorentzians are sufficient to fit the entire accessible Q/E range, as demonstrated in the manuscript and in Figure S3 below. To reliably separate the two processes, it is advantageous to constraint the fitting as described in the next section.

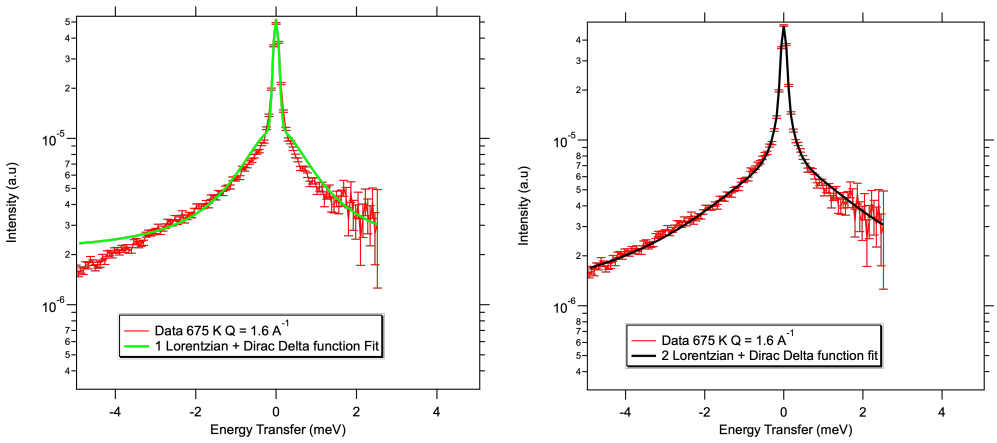


**Figure S3.** Comparison of QENS fits using a single Lorentzian (left) or 2 Lorentzians (right) to describe the quasi-elastic contribution.

**Quantitative fitting expression:** The minimal model that describes the QENS data in the $Cu_2Se$ superionic system is the δ-function elastic peak, in combination with two Lorentzian quasielastic components:

$$S(Q,\omega) = A(Q)\delta(\omega) + \left(1 - A(Q)\right)L_1(\omega) + L_2(\omega, Q) \quad (3)$$

The first Lorentzian $L_1$ represents the localized, confined "jump-diffusion" around an average position:

$$L_1 = \frac{\left(\frac{\Gamma_1}{2}\right)^2}{\pi\left[\omega^2 + \left(\frac{\Gamma_1}{2}\right)^2\right]} \quad (4)$$

It is well known that this type of confined diffusion leads to a FWHM ( $\Gamma_1$ ) that is essentially independent of $Q^2$ [30]. As the particle sporadically returns to its original position, there is an elastic incoherent structure factor contribution given by $A(Q)$ which depends on the confinement geometry. As a first approximation, the relation for a sphere with radius $a$

can be used since the deviation from this will be small at low Q for any more complex geometry [30]:

$$A\left(Q\right) = \left[\frac{3j_1\left(Qa\right)}{Qa}\right]^2$$

(5)

where $j_1$ is the n=1 spherical Bessel function [31, 32]. In practice the fitting procedure can also leave *A(Q)* as a free parameter determined at each *Q*. This is the approach used in our work. Figure S4 compares the measured EISF with Equation 5 for the $Cu_2Se$ data at 675 K showing the results are very similar. The second Lorentzian accounts for long-range diffusion and has a *Q*-dependent energy-width ($\Gamma_D$):

$$L_2 = \frac{\left(\frac{\Gamma_D}{2}\right)^2}{\pi(\omega^2 + \left(\left(\frac{\Gamma_D}{2}\right)\right)^2}$$

(6)

Thus, unlike $\Gamma_1$ which is common to all Q points, $\Gamma_D$ is a free parameter determined at each Q value. It is important to recognize that this model is different from those of both Danilkin *et al.* [8] and Voneshan *et al.* [3] because it explicitly models the confined diffusion as a Lorentzian with Q-independent width. The fits to this simple model are excellent, as shown in Figs. 7(a) and 7(b) in the main manuscript. The fitting was achieved using a 2D fit to minimize the global figure-of-merit $\chi^2$ by iterating $\Gamma_1$ through a set of values whilst allowing $\Gamma_D$ to fit freely at each value. The results are discussed in the main manuscript.

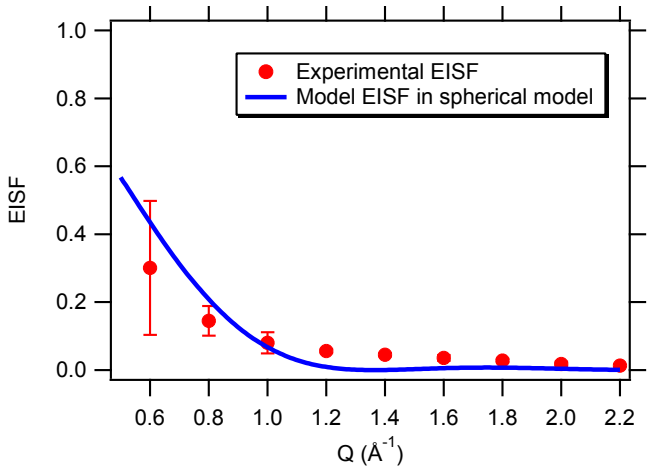


**Figure S4**. Measured EISF compared with the EISF estimated from a simple spherical model with a = 3.3 ± 0.2 Å

**Extracting the long-range diffusion component:** Provided the localized QENS component is accounted for properly, as described above, the Q-dependence of the second Lorentzian component is the key to detecting the diffusion coefficients. Different types of long-range diffusion (Hall-Ross, Fickian and Chudley Elliot) will lead to some variation in the Q-dependence at higher Q. In the case of the $Cu_2Se$ system, neither the Fickian model (which describes the free diffusion such as in water), nor the Hall-Ross Model (which describes a fully random set of short-range of jumps with a Gaussian distribution) capture the Q-dependency of the $\Gamma_D$. Instead, in agreement with past work [3], the Q-dependence is well described by the Chudley-Elliot (CE) model which describes long-range diffusion by discrete jumps between distinct crystallographic sites with a characteristic spacing. In the CE model, the FWHM from the diffusive component is:

$$\Gamma_D = \frac{2\hbar}{\tau}\left(1 - \frac{\sin(Qd)}{Qd}\right) \quad (2)$$

where $\tau$ is the hopping time, and $d$ is the hopping length and the diffusion coefficient is $d^2/6\tau$. Fig. 7 (a) shows a plot of the behavior of the CE model, within the experimental $\omega/Q$ range using d = 2 Å and d = 3 Å corresponding to T↔O and T↔T transitions respectively. The

most convincing method to clarify whether one of the latter hopping types dominates would be to observe a maximum in $\Gamma_D$ at $Qd = \frac{3\pi}{2}$ and the first minima in at $Qd = \frac{5\pi}{2}$. However, this is outside of the available experimental Q-range in $Cu_2Se$, so more approximate methods are needed. At very low Q, by taking the Taylor series of the CE model, one can see that $\Gamma_D \sim 2\hbar\, d^2/\tau$, and thus $d^2$ and $\tau$ parameters cannot be independently determined with a high level of precision, although the diffusion coefficient $d^2/6\tau$ is well resolved and for this reason the d = 2Å and d = 3Å collapse onto each other at low Q in Fig. 7. Meanwhile, at the other limit of extremely high Q, the CE model approaches a constant value of $\frac{2\hbar}{\tau}$ that is independent of *d*. The accessible Q-range in $Cu_2Se$ is somewhere between these limits, where the models are expected to show differences, albeit with a FWHM that approaches the experimental resolution (S4). For this reason, it is advantageous to establish the minimal model that can fit the data, and then use this to place broad upper and lower limits on the diffusion coefficients.

.

**Placing bounds on the data:** There are solid physical grounds to expect both O↔T and T↔T hops, but from the QENS data alone it is difficult to separate these two types of motion as both have similar jump lengths and hopping timescales and so will yield a similar $\Gamma_D$, thus potentially appearing as a single Lorentzian. As the diffusion coefficient determination depends, to some extent the ratio of O↔T to T↔T hops, we have developed a procedure to place bounds on the data assuming some distribution of hops. We assume that for two Lorentzians with the same width, within or near the resolution limit, these will appear as a single Lorentzian with an intensity that is the average of the two constituent Lorentzians, where the area under each Lorentzian is weighted by the fraction of each component. This allows assumption means that, for any fraction of different hops, the experiment will measure the intensity-weighted average (shown for example in Fig.S4) which always lies in the area between two single-Lorentzian limits obtained by assuming that 100% of either O↔T or T↔T hops. Importantly, although the true value will be in this region, it may not necessarily appear at the mid-point, even if the ratio was 50:50 However, provided the single-Lorentzian

data bounds all of the data, the true average will be included somewhere in the area bounded by the two curves. This allows one to place upper and lower limits.

To illustrate this, Fig. S4 (a) shows a plot of the behavior of the CE model, within the experimental $\omega/Q$ range using d = 2 Å and d = 3 Å corresponding to T↔O and T↔T transitions respectively.

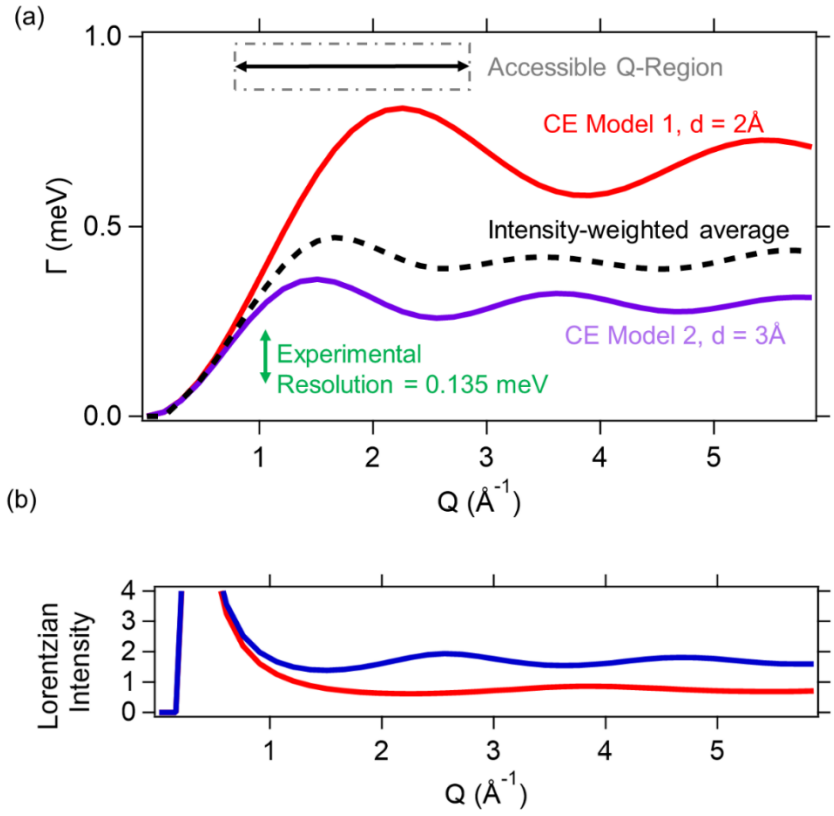


**Fig. S5.** (a) Plots of the Lorentzian width for the Chudley-Elliot model with two sets of parameters with d = 2 Å and d = 3 Å, chosen to give the same diffusion coefficients $d^2/6t$. The region of Q/E accessible in the experiment is shown in shaded region, along with the energy resolution. Within resolution the two models will have the same FWHM. Assuming both types of hops coexist with the same likelihood, the dotted line shows the apparent average width weighted by the intensity of each Lorentzian. (b) The apparent intensity of each Lorentzian in the model assuming that the intensity is inversely proportional to the FHWM so that the integrated area under each Lorentzian is constant.